Supplementary Information

Uncovering Gamma-Stable Organic Semiconductors: Large-Scale Screening and Predictive Modelling for Radiation-Hard Applications

Authors:

Andreas J. Bornschlegl[1*], Attila J. Mozer[2*], Jessie A. Posar[3], Jianchang Wu[1,4], Juan S. Rocha-Ortiz[1,4], Patrick Duchstein[5], Mauricio Caicedo-Reina[6], Alejandro Ortiz[6,7], Braulio Insuasty[6,7], Dirk Zahn[5], Justin B. Davies[8], Marco Petasecca[3], Larry Lüer[1,4,9*], Christoph J. Brabec[1,4,9,10*]

* Corresponding authors:

Andreas J. Bornschlegl: andreas.bornschlegl@fau.de

Attila J. Mozer: attila@uow.edu.au

Larry Lüer: larry.lueer@fau.de

Christoph J. Brabec: christoph.brabec@fau.de

Affiliations:

[1]Institute of Materials for Electronics and Energy Technology (i-MEET), Department of Materials Science and Engineering, Friedrich-Alexander-Universität Erlangen-Nürnberg (FAU), Martensstraße 7, 91058 Erlangen, Germany

[2]Intelligent Polymer Research Institute and ARC Centre of Excellence for Electromaterials Science, University of Wollongong, Wollongong, New South Wales 2522, Australia

[3]Centre for Medical Radiation Physics, University of Wollongong, Wollongong, NSW, 2522 Australia

[4]Helmholtz-Institute Erlangen-Nürnberg for Renewable Energy (HI ERN), Forschungszentrum Jülich GmbH, Immerwahrstraße 2, 91058 Erlangen, Germany

[5]Chair for Theoretical Chemistry / Computer Chemistry Center (CCC), Department of Chemistry and Pharmacy, Friedrich-Alexander-Universität Erlangen-Nürnberg (FAU), Nägelsbachstraße 25, 91052 Erlangen, Germany

[6]Heterocyclic Compounds Research Group, Department of Chemistry, Universidad del Valle, Calle 13 #100-00, 25360, Cali, Colombia

[7]Center for Research and Innovation in Bioinformatics and Photonics-CIBioFi, Calle 13 #100-00, Edificio E-20, No. 1069, 25360, Cali, Colombia

[8]Australian Nuclear Science and Technology Organisation, Lucas Heights, Australia

[9]FAU Profile Center Solar, Friedrich-Alexander University Erlangen-Nürnberg, Erlangen, Germany

[10]IMD-3 Photovoltaics, Forschungszentrum Jülich GmbH, 52428 Jülich, Germany

Materials and Methods

Material Synthesis

The materials A18B1, A31B4, A30B6, A31B6, A32B6, A32B7, A30B8, A32B8, A33B8, A33B9, A32B11, A33B12, A1087B3, A1090B3, A30B770, A1106B770, A1100B10, A1066B12, A1087B2, A1090B6 were synthesized as previously described by Wu et al.[1,2]

The synthesis of TM-1 and TM-4 is described by Rocha-Ortiz et al.[3] PyBDP-1, PyBDP-2, PyBDP-3, PyBDP-4, and PyBDP-5 were synthesized as previously explained by Seoneray et al.[4] The synthesis of the materials TMF-2, MCR-276, MCR-284, MCR-397, MCR-403, and MCR-428 is presented in the work by Caicedo-Reina et al.[5,6]

The commercial materials were purchased from the following companies: HTL-B (Sigma-Aldrich, TCTA), HTL-C (TCI, 1,3,5-Tris[4-(9-carbazolyl)phenyl]benzene), TPA-BCN (BLD, 4',4''',4''''-Nitrilotris(([1,1'-biphenyl]-4-carbonitrile))).

Sample Preparation

For each material in this work, a 3 mg/ml solution in chloroform (Sigma-Aldrich) was prepared and stirred overnight at 300 rpm and 60°C (BioShake 3000, Qinstruments). The 25 mm x 25 mm glass substrates were cleaned in an ultrasonic bath with DI water, acetone, and IPA for 10 minutes each. Afterwards, the substrates were treated with UV-ozone for 20 minutes. The thin films were spin-coated (static, 50 ul, 600 rpm, 5000 acc.) onto the substrate using a spin-coating robot (SpinBot, Sciprios) and annealed at 120°C for 2 minutes at ambient conditions. The outer edges of the thin films were wiped off with cotton tips submerged in ethanol to make space for the later encapsulation. The samples were packaged in three layers of 150 µm thick vacuum bags (CASO) using a vacuum sealer (VC10, CASO) inside the glovebox and shipped to Australia within less than 5 days. The sealing was done by placing a gasket (Surlyn 25 µm thick, Dyenamo) onto the rim of each sample and pressing a glass substrate from the top onto the sample while the sample is on a hot plate (110°C). The process took around 2 minutes for each sample and was performed in an argon-filled glove box. It was made sure that both the bottom and top substrate were from the same glass batch. The effectiveness of the sealing in maintaining an inert atmosphere can be seen in Figure S2.

Gamma Degradation & UV-vis Characterization

The gamma degradation was carried out at the Australian Nuclear Science and Technology Organisation (ANSTO) with a cobalt-60 (1.17 MeV, 1.33 MeV) batch type irradiator. The films were placed in a Perspex phantom, with designated slots in a single layer, oriented vertically and parallel to the source array (Figure S3). The phantom had a 10 mm thick Perspex cover (radiation build-up material) that provided approximate charged particle equilibrium to the films during exposure to gamma radiation. The dose rate was approximately 1 kGy/h, measured using Fricke dosimeters (ISO/ASTM 51026).[7] Before, during, and after degradation, ex-situ UV-vis measurements of the samples and reference stacks were performed with a fiber-coupled spectrometer (between 1 and 2 ms integration time, 300 to 500 averages, Jaz, Ocean Optics). A 450 W Xe lamp (CX-04E, Inotech, Japan) was used as a light source.

Data Processing

The glass batch-dependent color centers forming during gamma degradation were corrected by subtracting the absorbance of the reference stack from the sample while making sure that the glass batches match (Figure S4, Figure S5, Figure S6). The baseline of the UV-vis spectra was corrected by subtracting a linear fit to the tail from the spectrum (Figure S7, Figure S8, Figure S9). The degradation was monitored by fitting a Gaussian to the π-π* band of each material, tracking the peak absorbance with accumulated gamma-ray dose (Figure 1c, Figure 1d, Figure S10). [8] For the fit, a hyperbolic formula trained on organic solar cell degradation data via symbolic regression as explained by Song et al. was chosen:

$$y(a,b,d) = 1 - \frac{d(2d + \sqrt{b+1})^b}{b},$$

where d is the gamma dose in Gray (Gy). For a and, b the bounds (100, 1e6) and (-0.6, 0.2) were chosen, respectively.

The accumulated energy dose (AED_{90}) – acting as a stability target for gamma-ray degradation – was extracted by fitting the data – including the data of both films for the same material - and determining the dose at 90% of the initial peak absorbance (Figure S10, Table S1). In case the peak absorbance never decreased below 90%, the curve was linearly extrapolated. In cases where linear extrapolation did not intersect y=90% at a reasonable dose (see TM-1, TM-4 and PyBDP-2 in Figure S10), the AED_{90} was fixed to 1,000,000 Gy (Table S1), more than half an order of magnitude higher than the most stable material out of the rest of the materials (PyBDP-4). This was done as choosing finite targets is essential for predictive modelling.

Predictive Modelling

The predictive modelling was performed in analogy to our previous work on UVC stability based on Mordred and QikProp descriptors.[8–10] In the present work on gamma stability, RDKit features have been added to the descriptor set.[11] Furthermore, the ~1,900 descriptors are reduced to the top 30 before mRMR (minimum Redundancy Maximum Relevance)-embedded Gaussian Process Regression is started.

Supporting Tables and Figures

Material	AED_{90} (Gy)	$\log_{10}(AED_{90})$
A33B9	1239.3	3.09
A31B4	1334.3	3.13
TPA-OMe6	5277.2	3.72
A33B8	5944.2	3.77
HTM-3	6095.5	3.79
MCR-397	6140.3	3.79
HTM-A	6482.5	3.81
MCR-428	6660.2	3.82
HTL-B	8039	3.91
A32B6	8795.8	3.94
A1090B3	8803	3.94
HTM-1	9056.6	3.96
HTM-2	9491.5	3.98
TPA-BCN	9767.7	3.99
A32B8	11117.8	4.05
HTM-E	11668.8	4.07
A31B6	12231.8	4.09
A30B6	12334.3	4.09
A30B770	13667.7	4.14
A1066B12	13936.1	4.14
HTM-H	14034.3	4.15
A33B12	14525.6	4.16
HTM-4	15038.6	4.18
PyBDP-3	15126.9	4.18
MCR-284	15498.1	4.19
A1087B3	15610.63	4.19
TMF-2	16015.6	4.2
HTL-C	17351.8	4.24
A1100B10	17409.3	4.24
A1087B2	17658.8	4.25
A1090B6	17759.5	4.25
A32B7	19012	4.28
MCR-276	19133.7	4.28
A30B8	20013	4.3
A32B11	20683.2	4.32
A18B1	21750	4.34
PyBDP-1	22183.1	4.35
A1106B770	22683.9	4.36
A31B12	23998.3	4.38
A21B1	35600.7	4.55
MCR-403	42961.2	4.63
PyBDP-5	52554.8	4.72
PyBDP-4	321814.7	5.51
TM-1	1000000	6
TM-4	1000000	6
PyBDP-2	1000000	6

Table S1: Extracted stability target values (AED_{90}, $\log_{10}(AED_{90})$) of all materials sorted in ascending AED_{90} order.

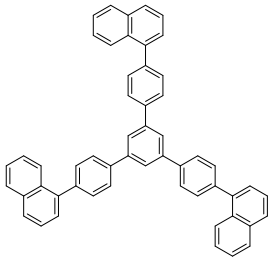

A33B9

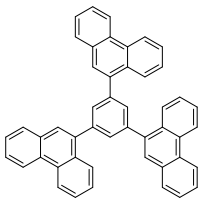

A31B4

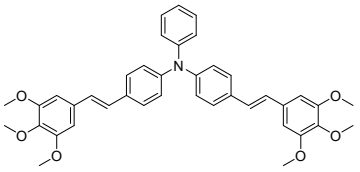

TPA-OMe6

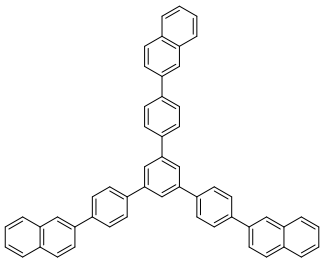

A33B8

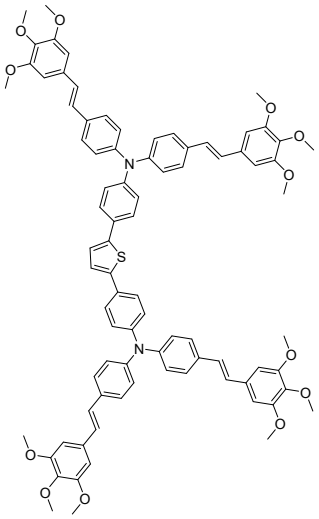

HTM-3

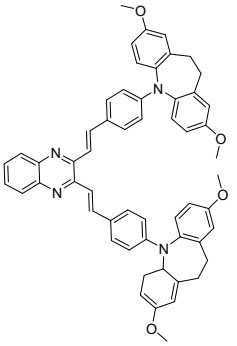

MCR-397

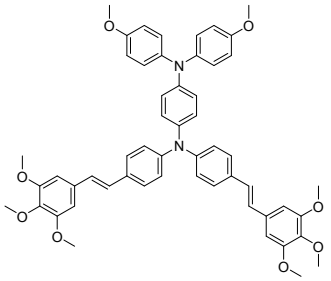

HTM-A

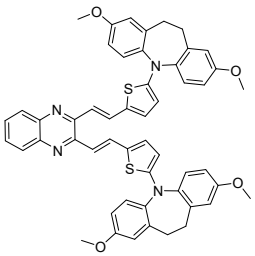

MCR-428

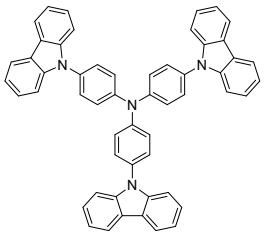

HTL-B

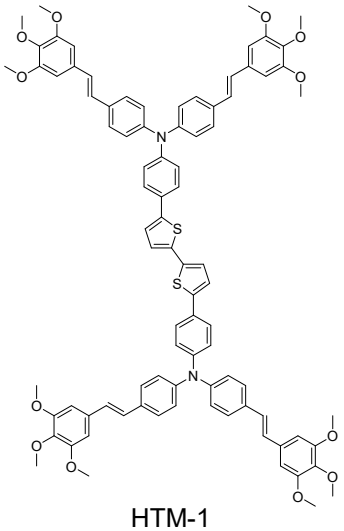

HTM-1

A32B6

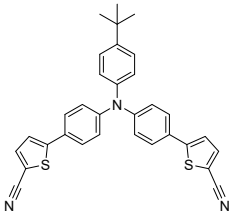

A1090B3

Figure S1: Chemical structures of tested materials sorted by ascending AED_{90} stability target.

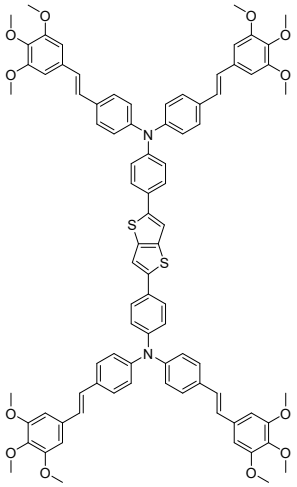

HTM-2

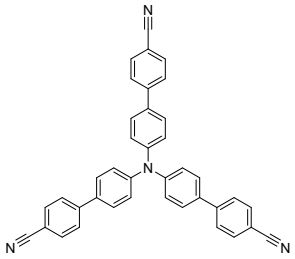

TPA-BCN

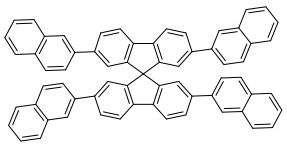

A32B8

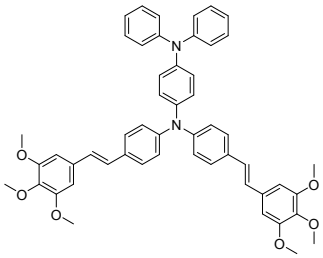

HTM-E

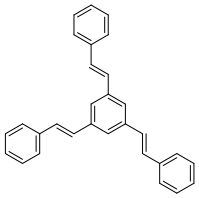

A31B6

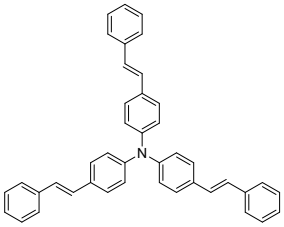

A30B6

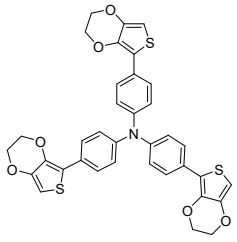

A30B770

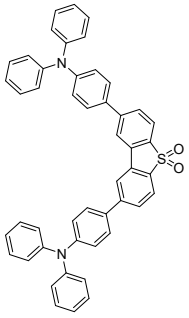

A1066B12

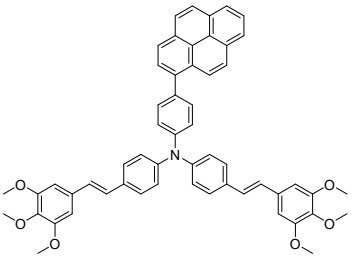

HTM-H

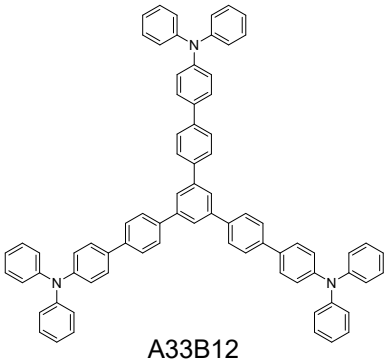

A33B12

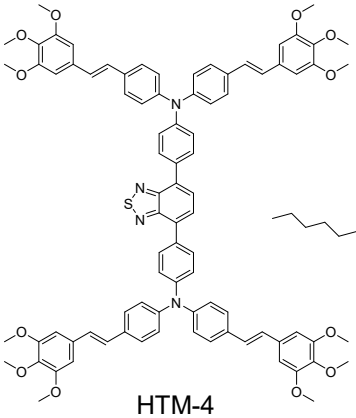

HTM-4

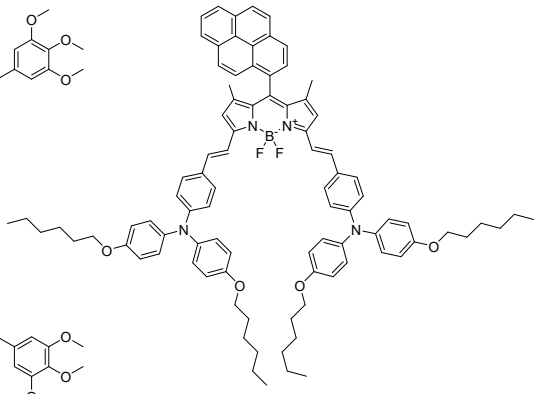

PyBDP-3

Figure S1: Chemical structures of tested materials sorted by ascending AED_{90} stability target.

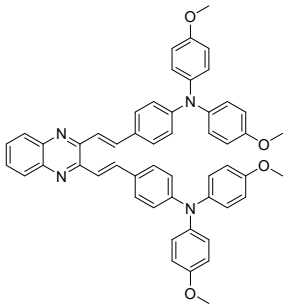

MCR-284

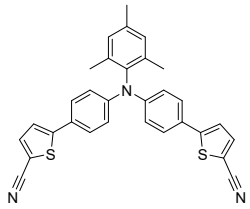

A1087B3

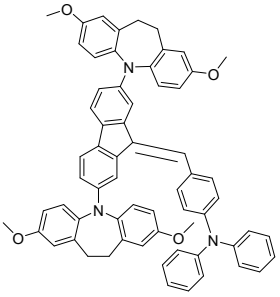

TMF-2

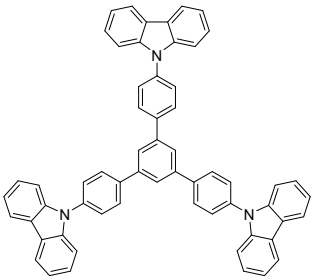

HTL-C

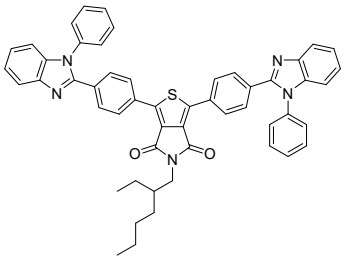

A1100B10

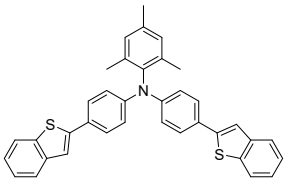

A1087B2

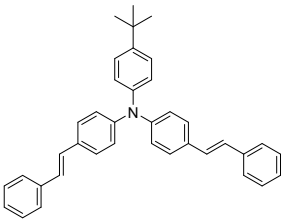

A1090B6

A32B7

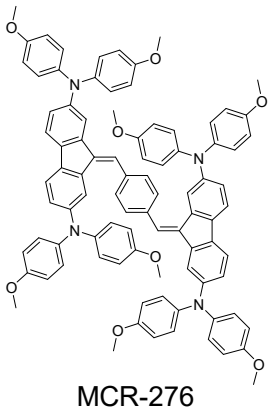

MCR-276

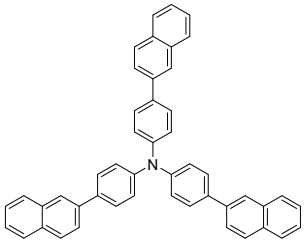

A30B8

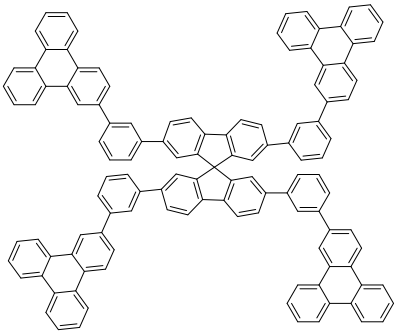

A32B11

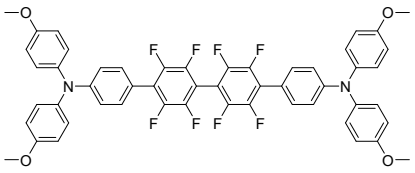

A18B1

Figure S1: Chemical structures of tested materials sorted by ascending AED_{90} stability target.

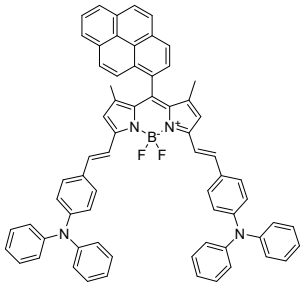

PyBDP-1

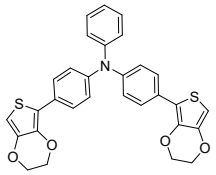

A1106B770

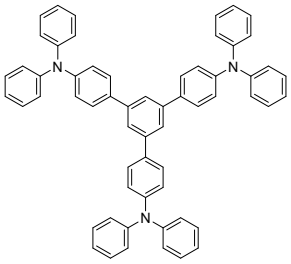

A31B12

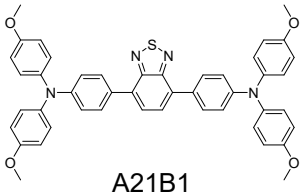

A21B1

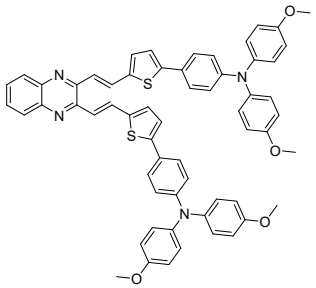

MCR-403

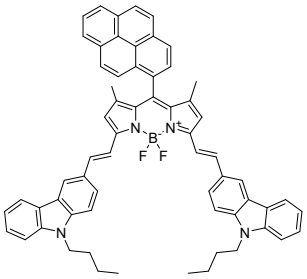

PyBDP-5

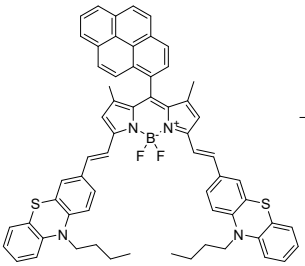

PyBDP-4

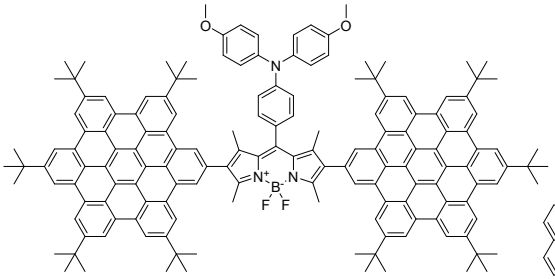

TM-1

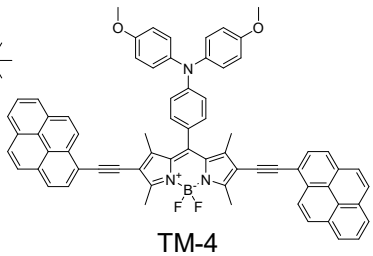

TM-4

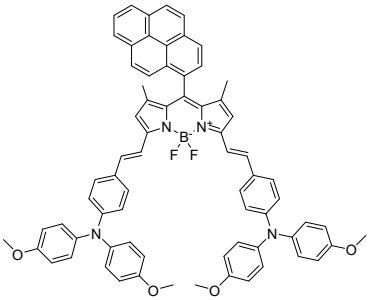

PyBDP-2

Figure S1: Chemical structures of tested materials sorted by ascending AED_{90} stability target.

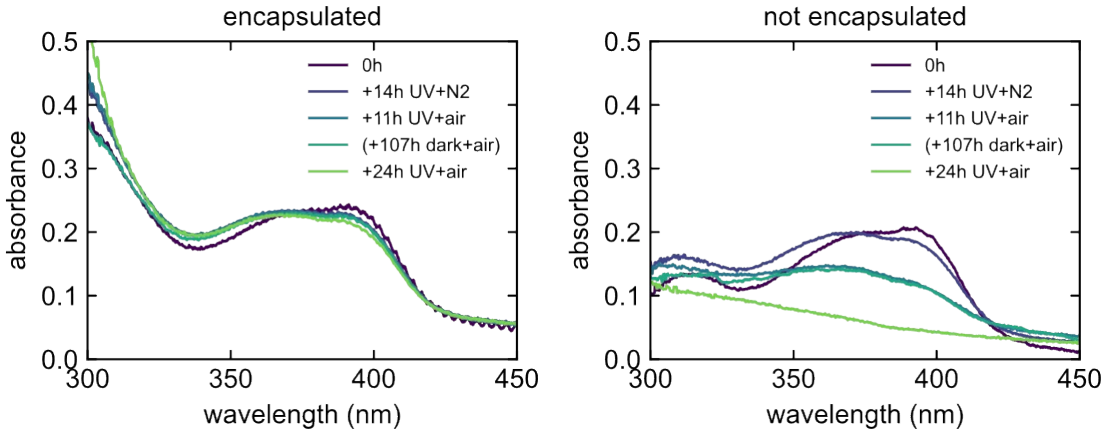

Figure S2: UV-vis spectra during UVC degradation of an encapsulated (left panel) vs. unencapsulated (right panel) Spiro-OMeTAD film. Turning off the nitrogen atmosphere does not affect the encapsulated sample.

Figure S3: Pictures of samples in the Perspex (PMMA) phantom before (left) and after (right) gamma degradation.

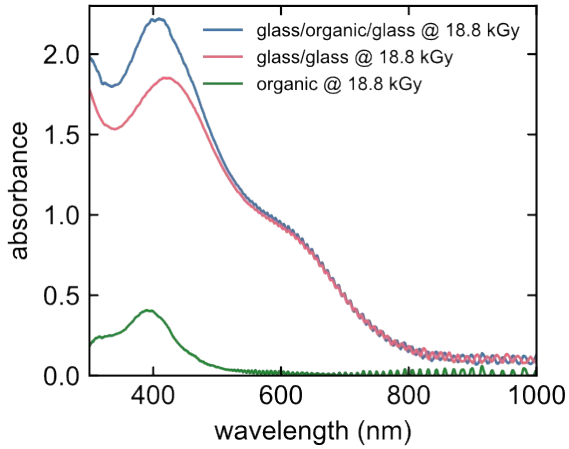

Figure S4: Revealing organic layer UV-vis @ 18.8 kGy (green curve) for HTM-2 by subtracting the reference stack (red curve) from the sample stack (blue curve).

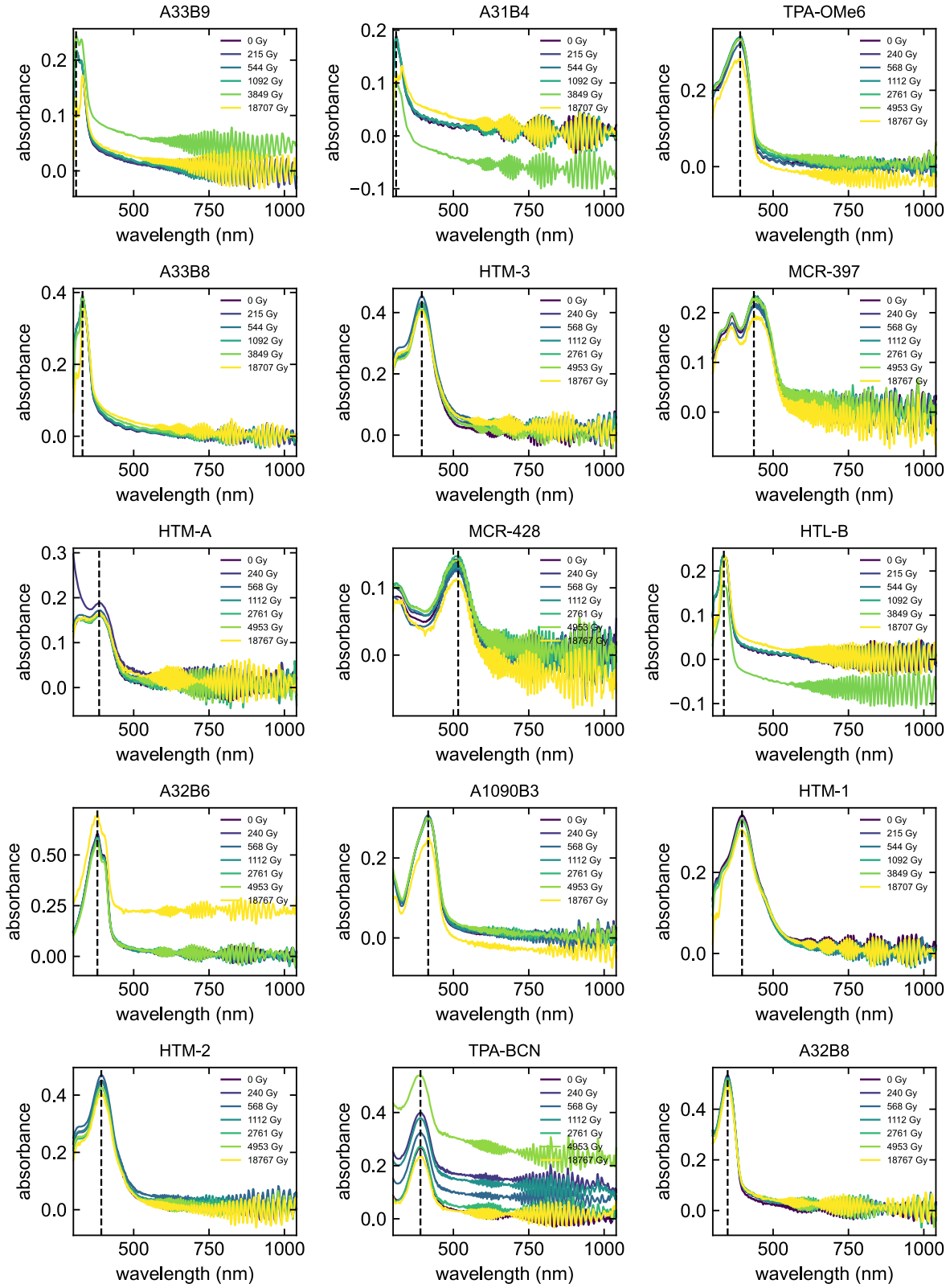

Figure S5: UV-vis evolutions of the first film of all materials after reference subtraction in ascending AED_{90} order. The black dashed lines shows the main peak of the spectrum used for AED_{90} extraction.

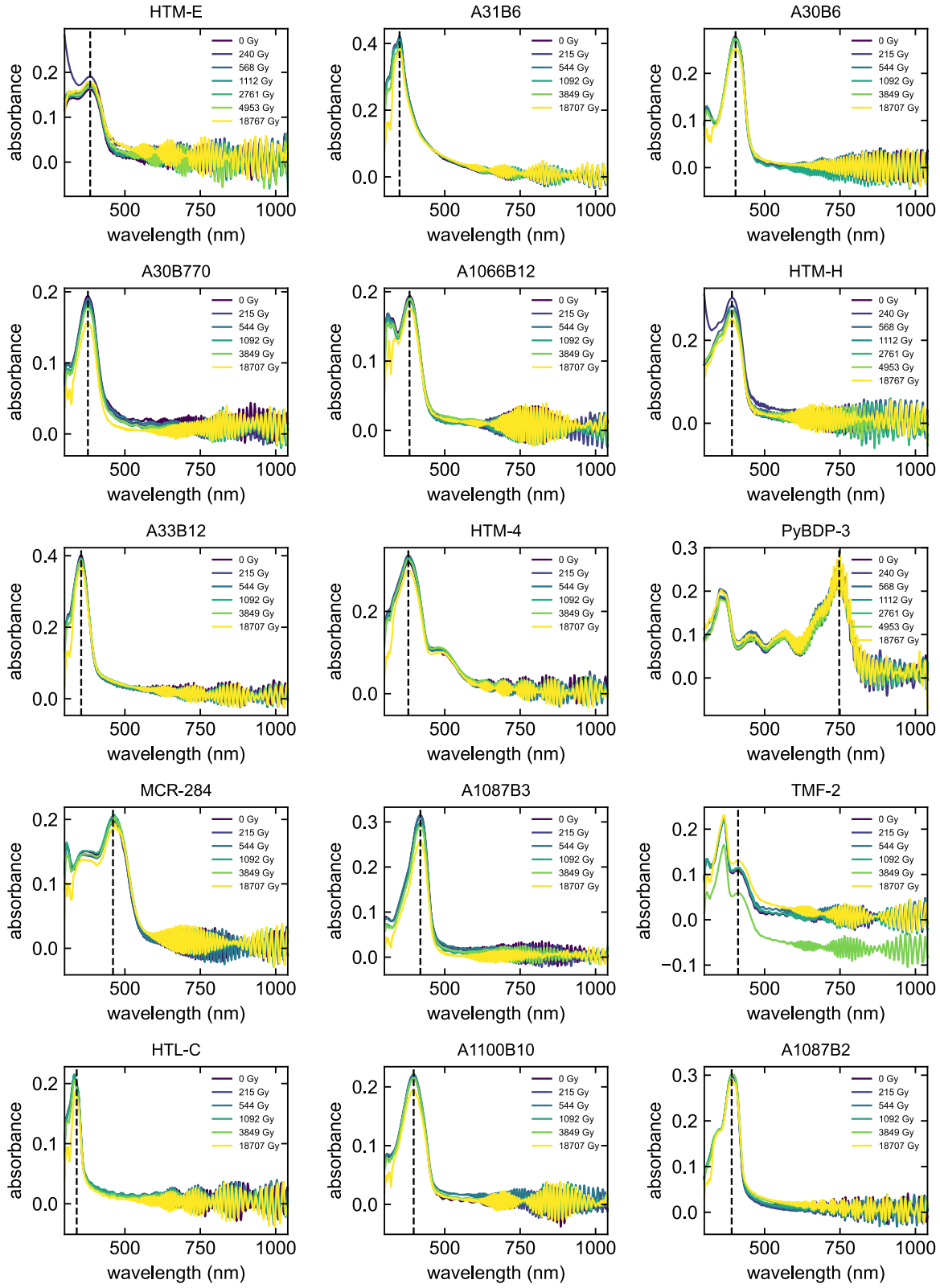

Figure S5: UV-vis evolutions of the first film of all materials after reference subtraction in ascending AED_{90} order. The black dashed lines shows the main peak of the spectrum used for AED_{90} extraction.

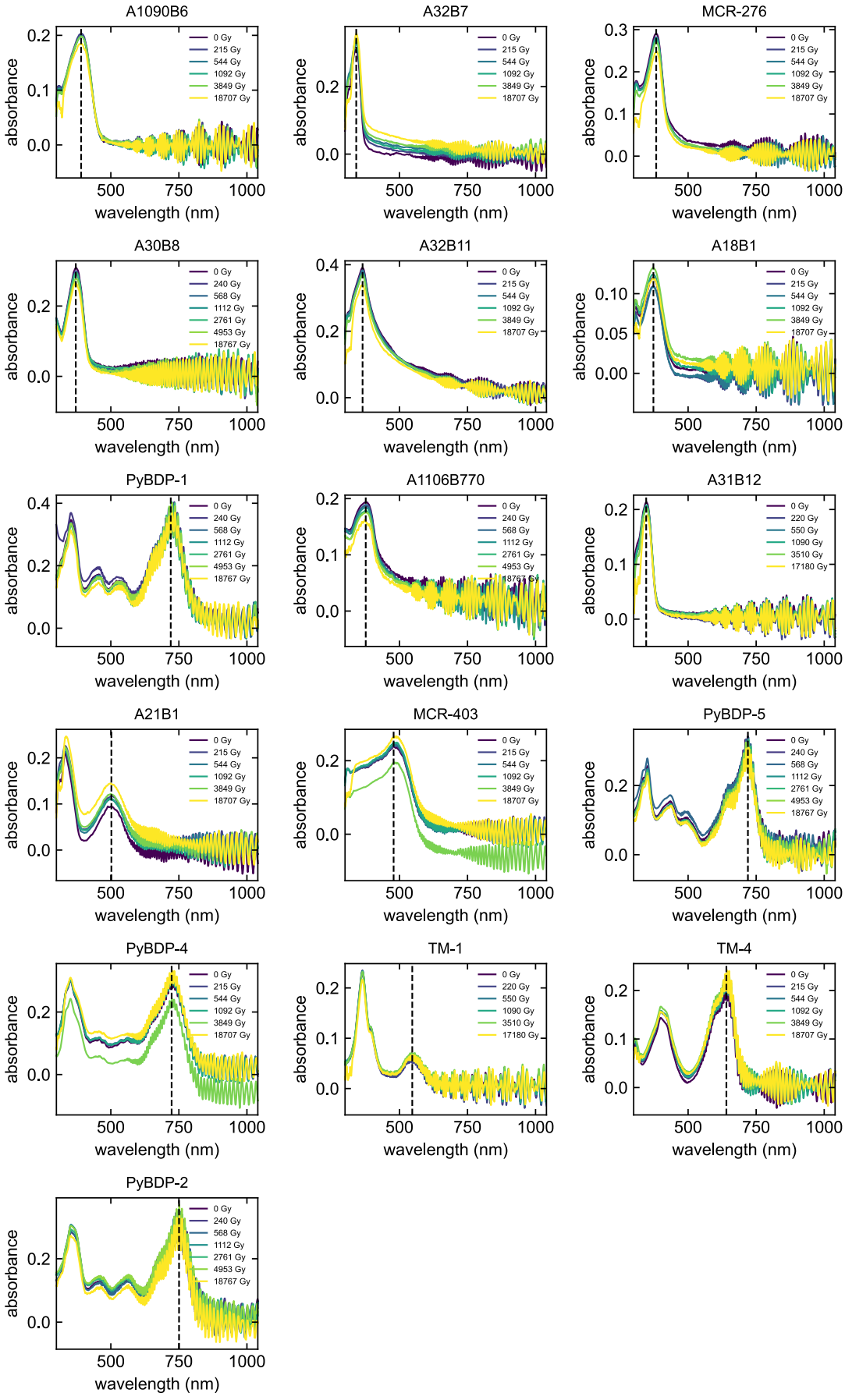

Figure S5: UV-vis evolutions of the first film of all materials after reference subtraction in ascending AED_{90} order. The black dashed lines shows the main peak of the spectrum used for AED_{90} extraction.

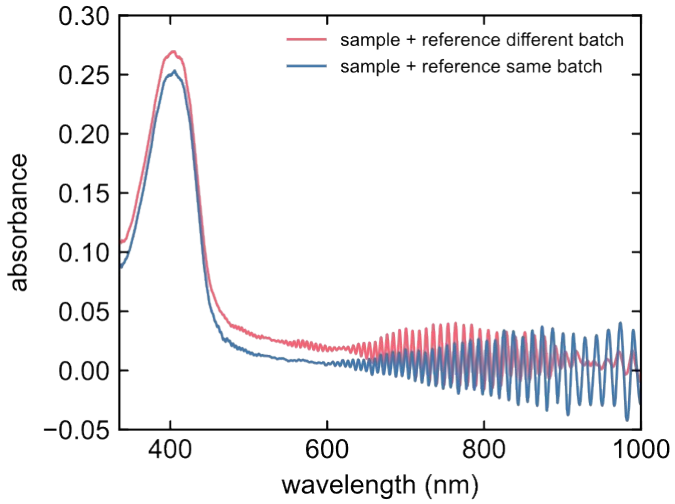

Figure S6: Example for sample (A30B6) corrected with reference stack of different glass batch (red curve) and same glass batch (blue curve).

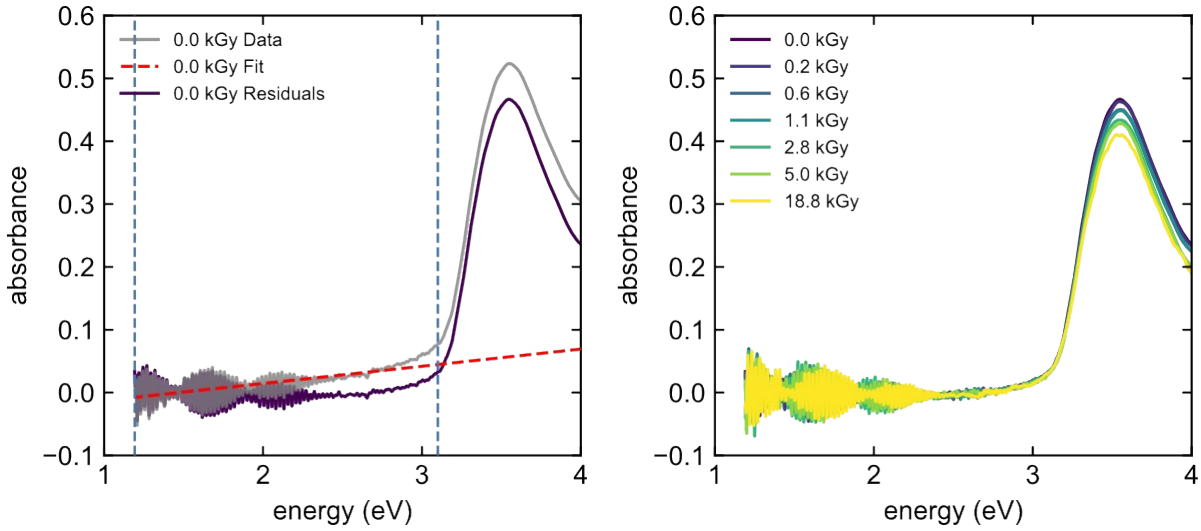

Figure S7: Subtraction of linear fit to tail from reference corrected UV-vis spectra (left), revealing a decreasing trend of the π-π band (right). The dashed blue lines show the energy interval of the linear fit (red dashed line).*

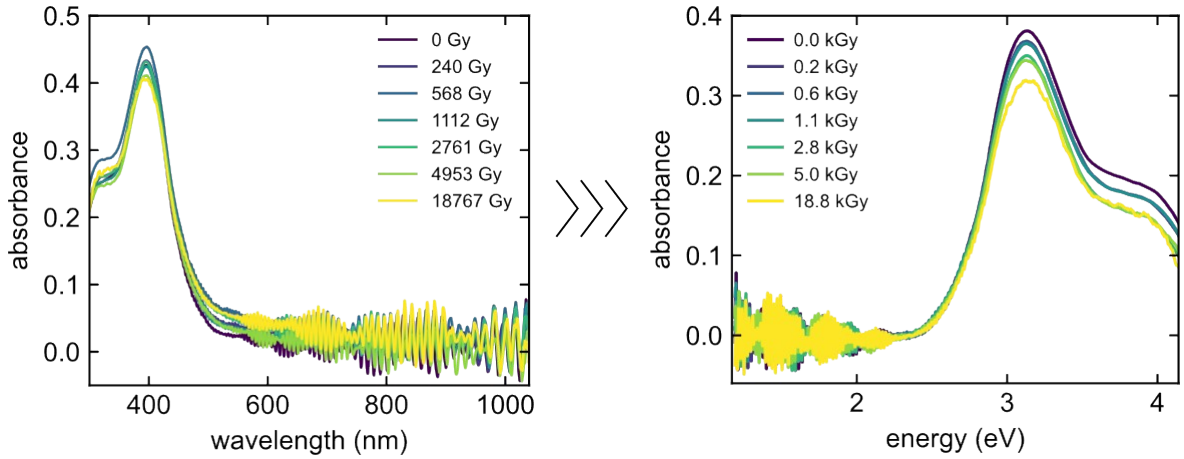

Figure S8: UV-vis spectra evolution before (left) and after (right) subtracting linear fit to the tail from the spectra, revealing a decreasing trend of the π-π band.*

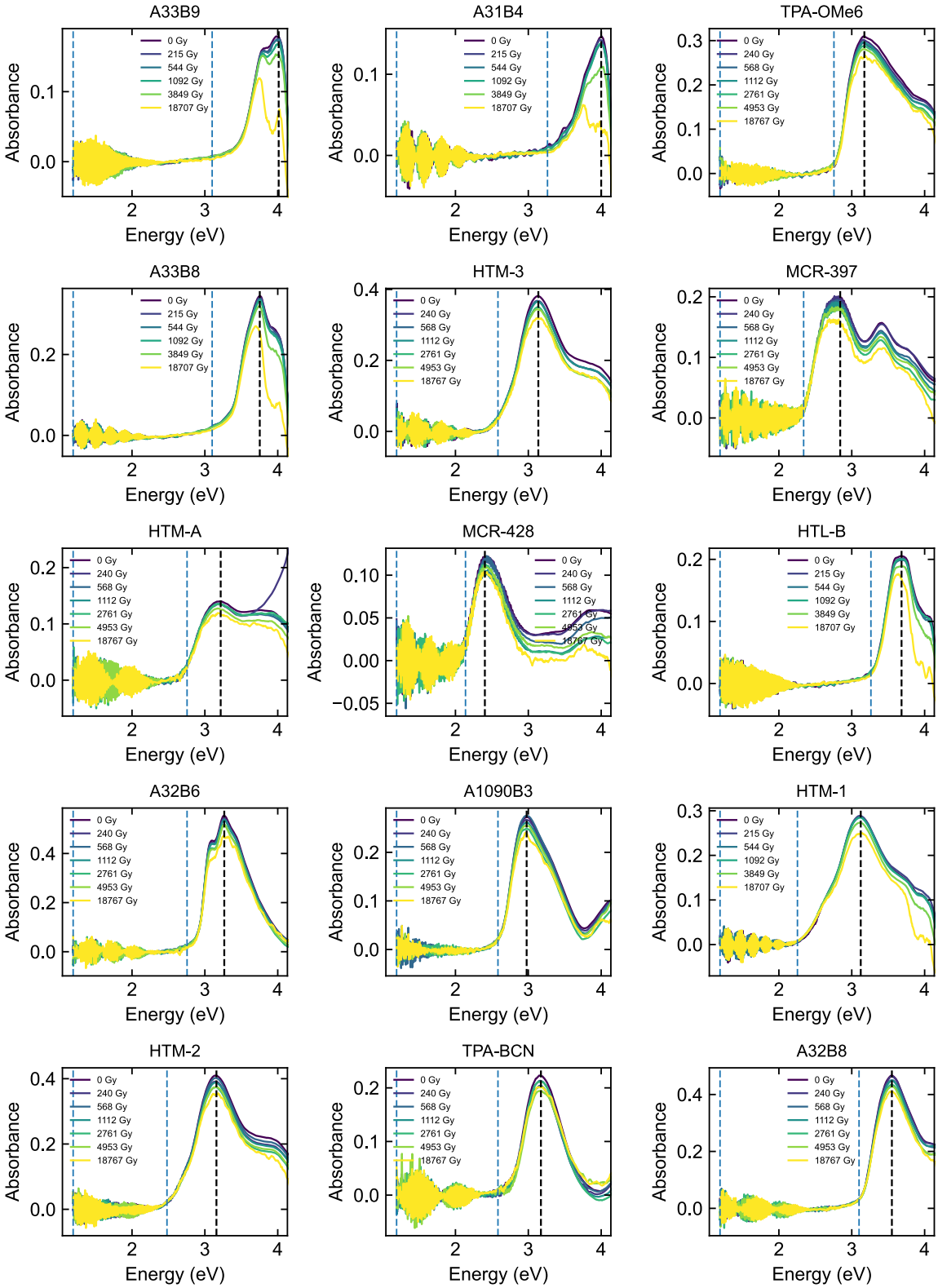

Figure S9: UV-vis evolutions of the first film of all materials after baseline correction in ascending AED_{90} order. The dashed blue lines show the energy interval of the linear fit correction. The AED_{90} is extracted from the main peak (black line).

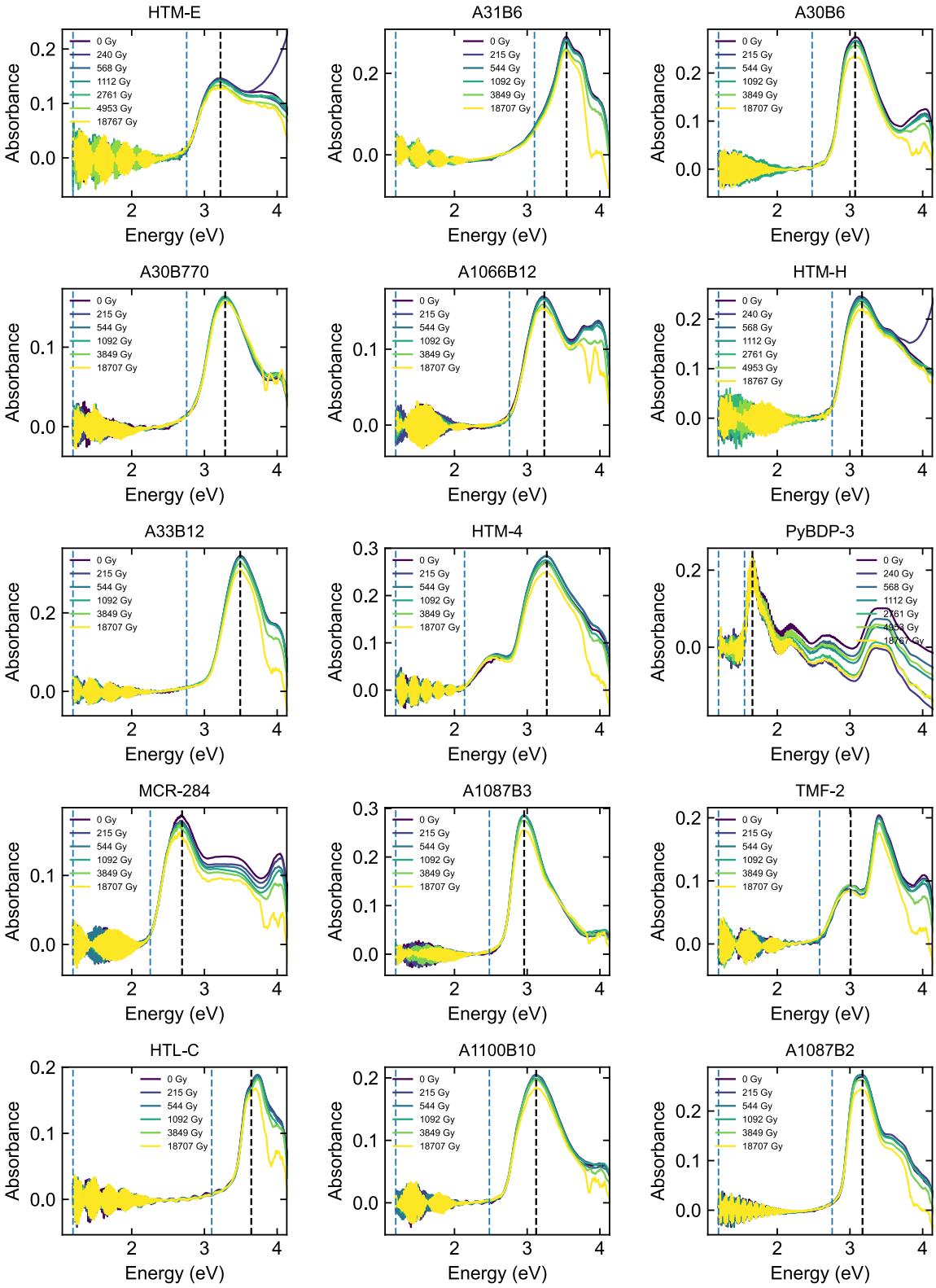

Figure S9: UV-vis evolutions of the first film of all materials after baseline correction in ascending AED_{90} order. The dashed blue lines show the energy interval of the linear fit correction. The AED_{90} is extracted from the main peak (black line).

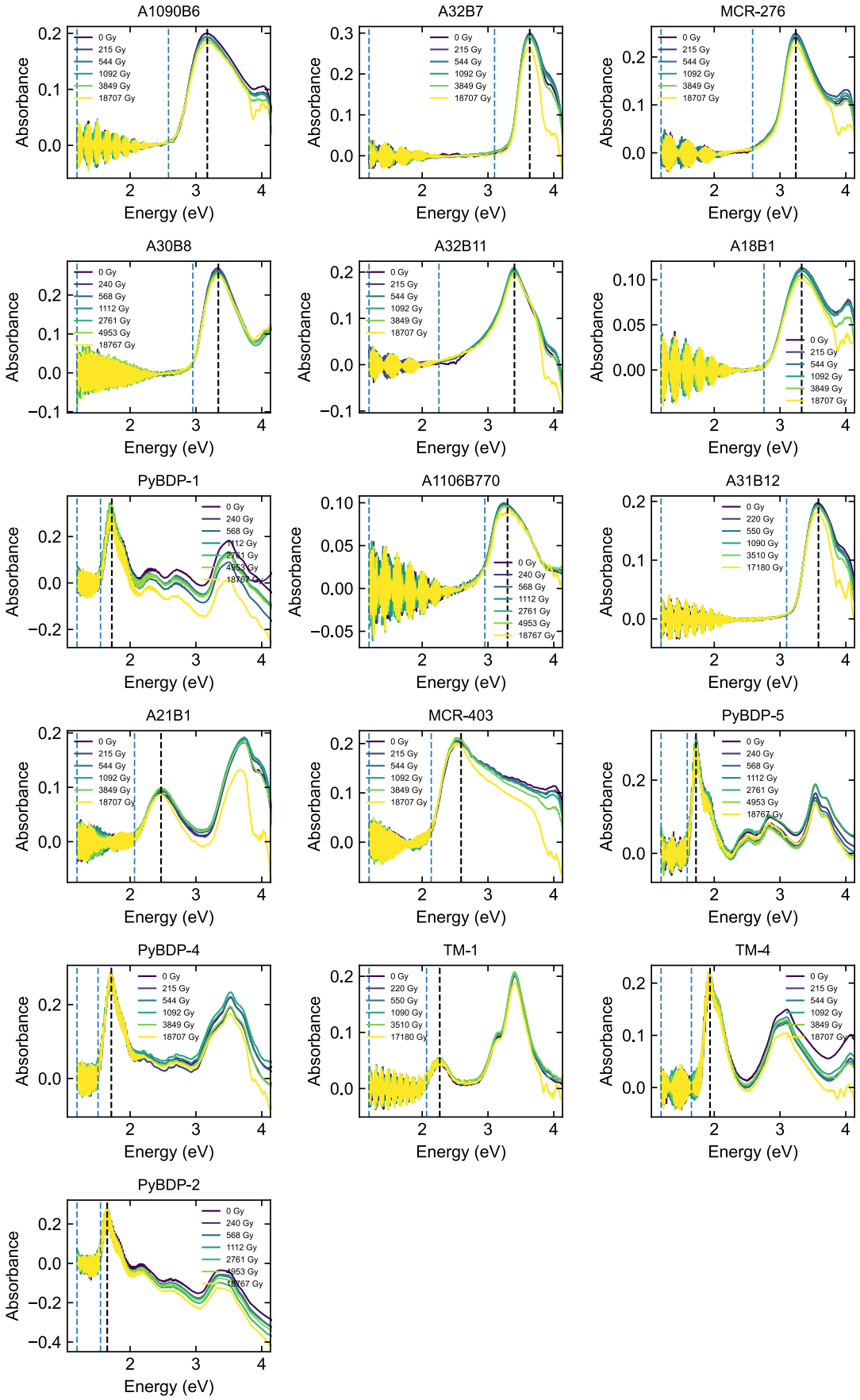

Figure S9: UV-vis evolutions of the first film of all materials after baseline correction in ascending AED_{90} order. The dashed blue lines show the energy interval of the linear fit correction. The AED_{90} is extracted from the main peak (black line).

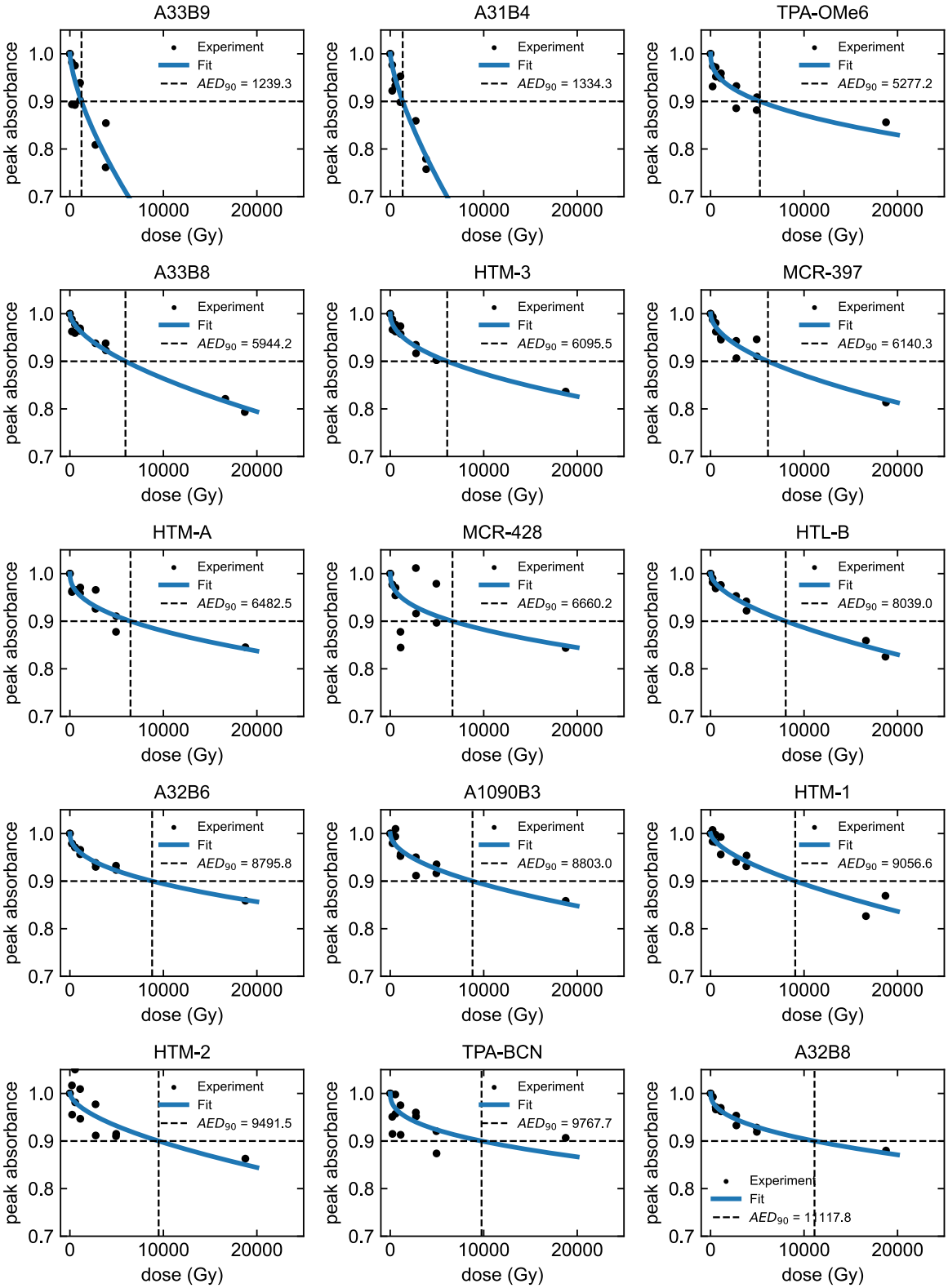

Figure S10: Fits of all π-π peak absorbance evolutions to extract the AED_{90} stability target in ascending AED_{90} order. If the fit does not intersect y=0.9, then it is linearly extrapolated.*

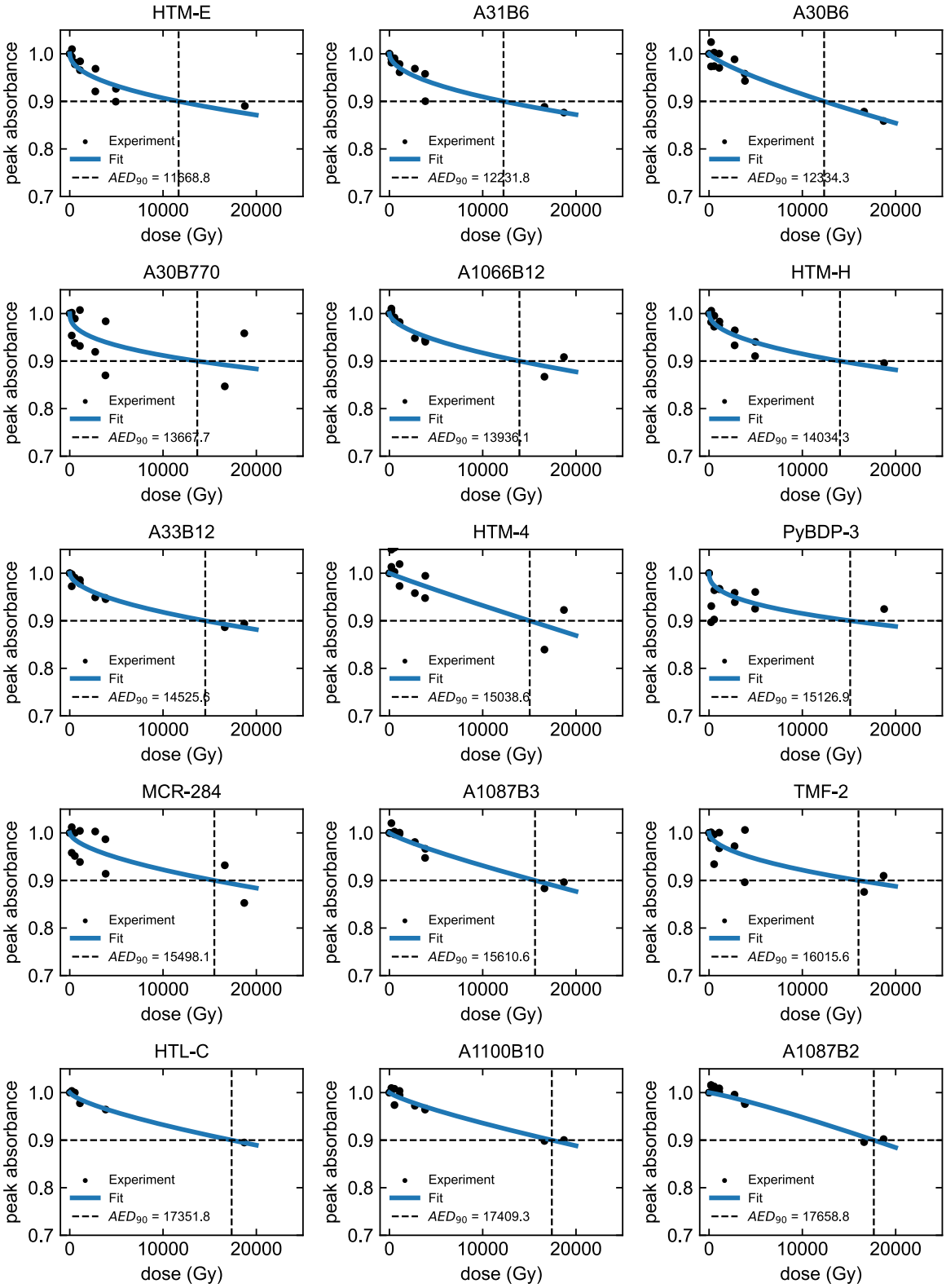

Figure S10: Fits of all π-π peak absorbance evolutions to extract the AED_{90} stability target in ascending AED_{90} order. If the fit does not intersect y=0.9, then it is linearly extrapolated.*

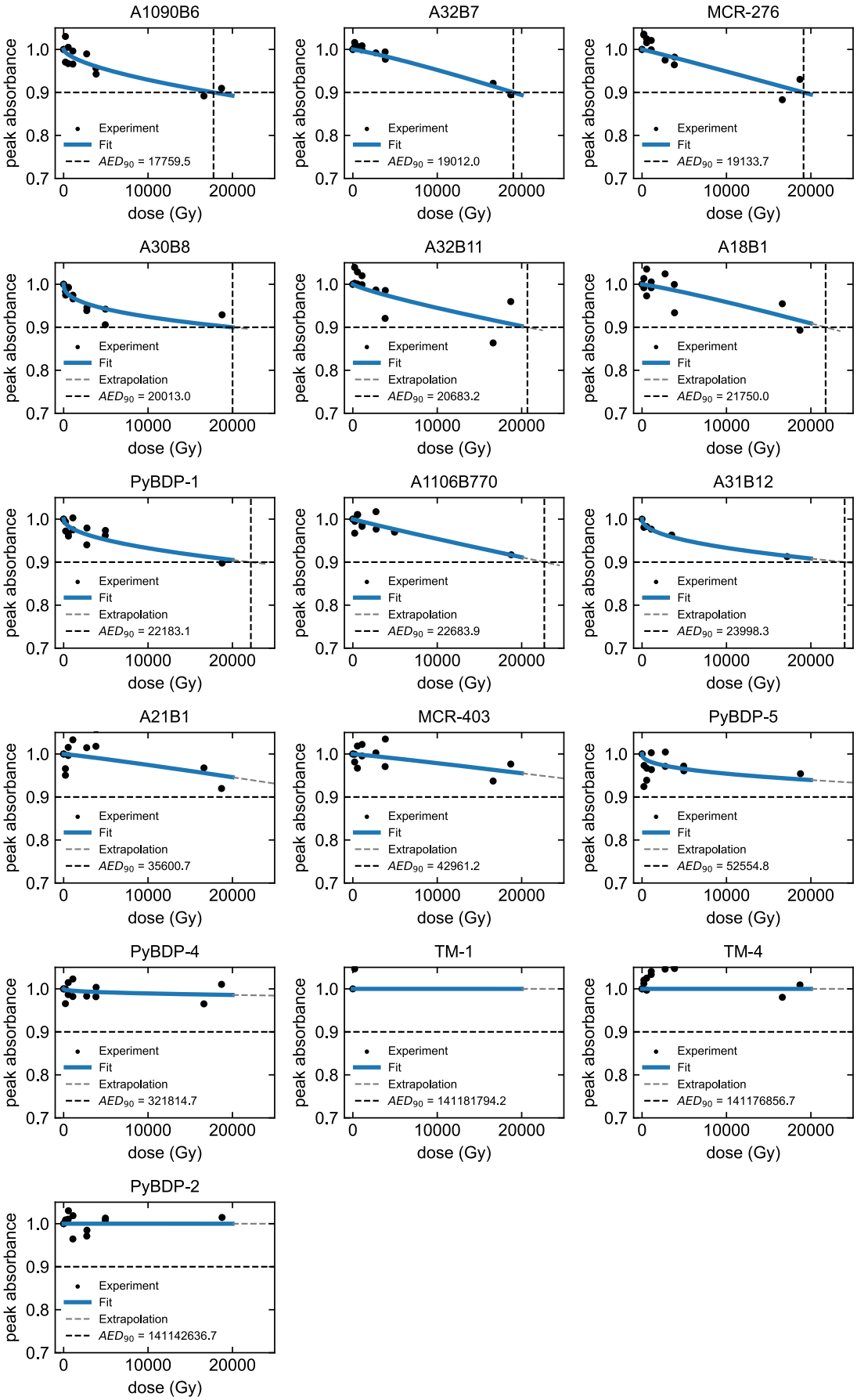

Figure S10: Fits of all π-π peak absorbance evolutions to extract the AED_{90} stability target in ascending AED_{90} order. If the fit does not intersect y=0.9, then it is linearly extrapolated.*

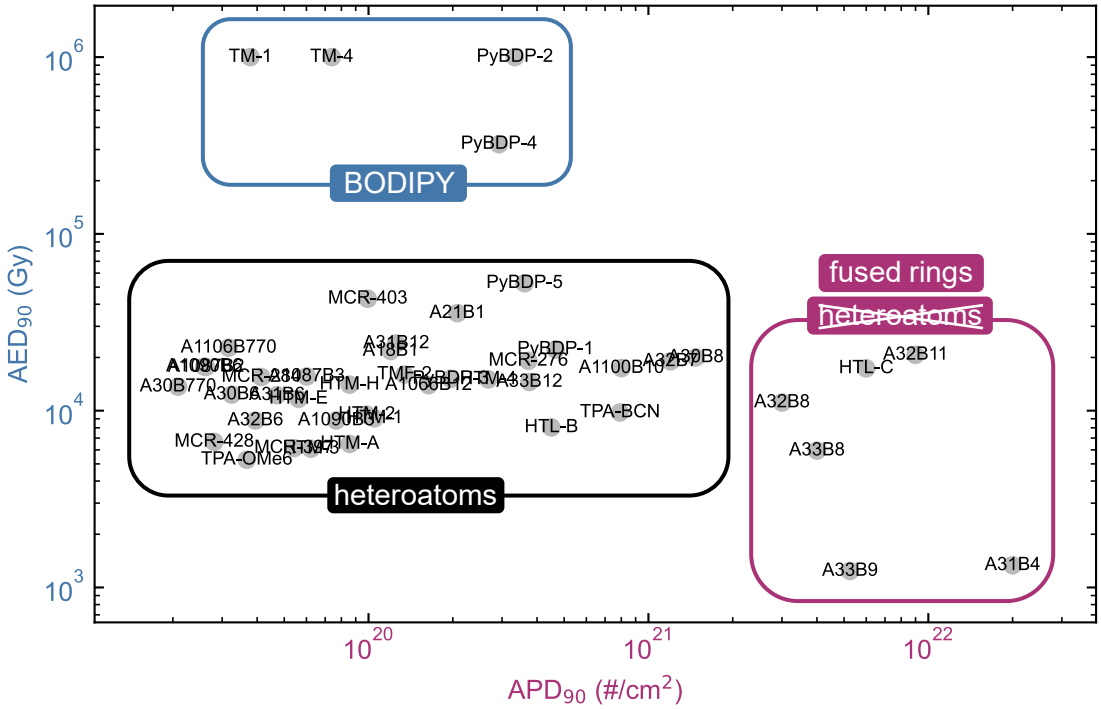

Figure S11: Gamma stability (AED_{90}) vs. UVC stability (APD_{90}) of the studied material library. UVC stable materials are gamma unstable and vice versa. The APD_{90} data is from a previous publication on UVC stability of the same materials.[8] The three clusters group the materials in general categories referred in the present work and in the work on UVC stability. Not all materials visually inside the clusters actually belong to them.

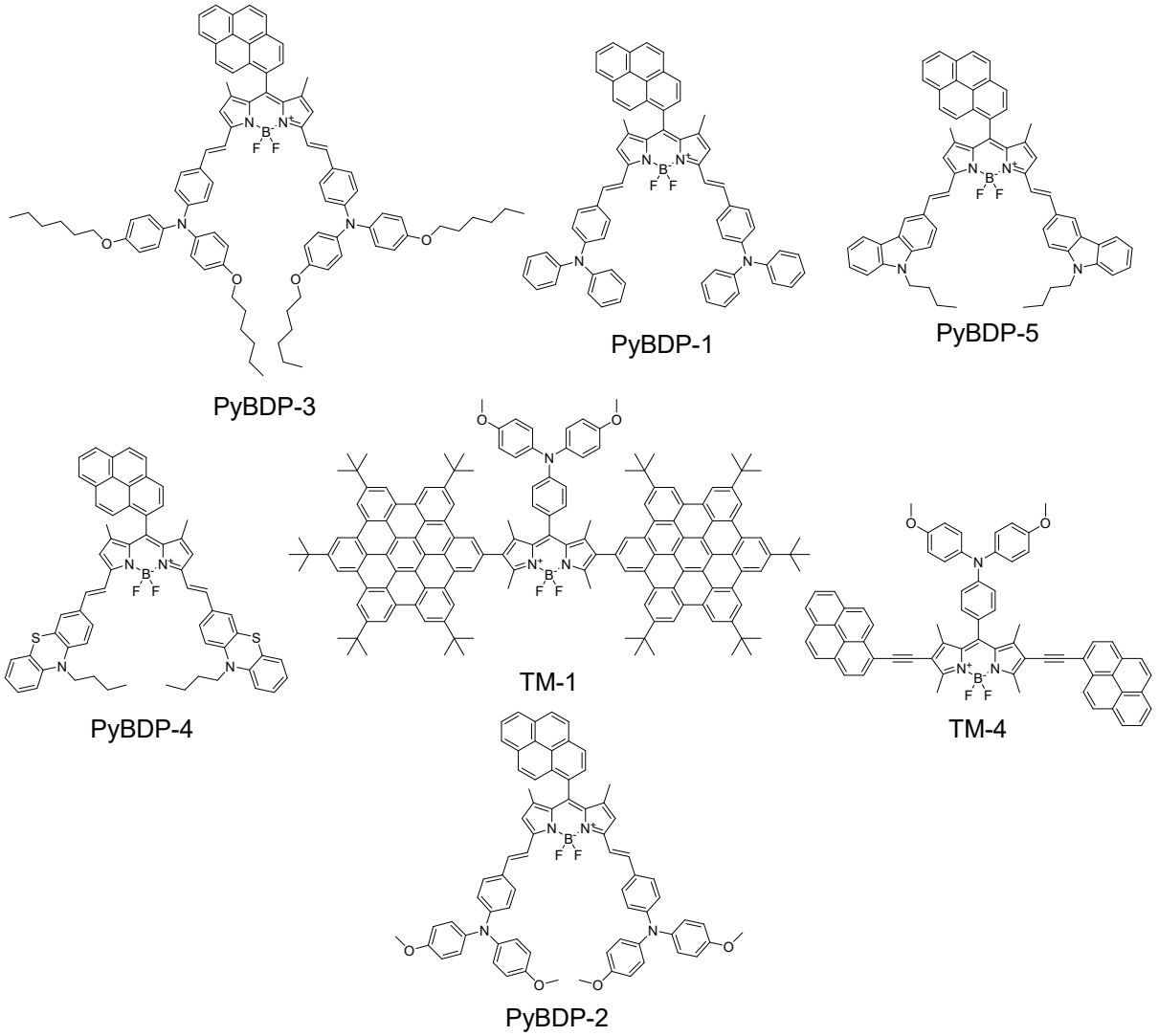

Figure S12: Chemical structures of all BODIPY derivatives sorted left to right in ascending AED_{90} order.

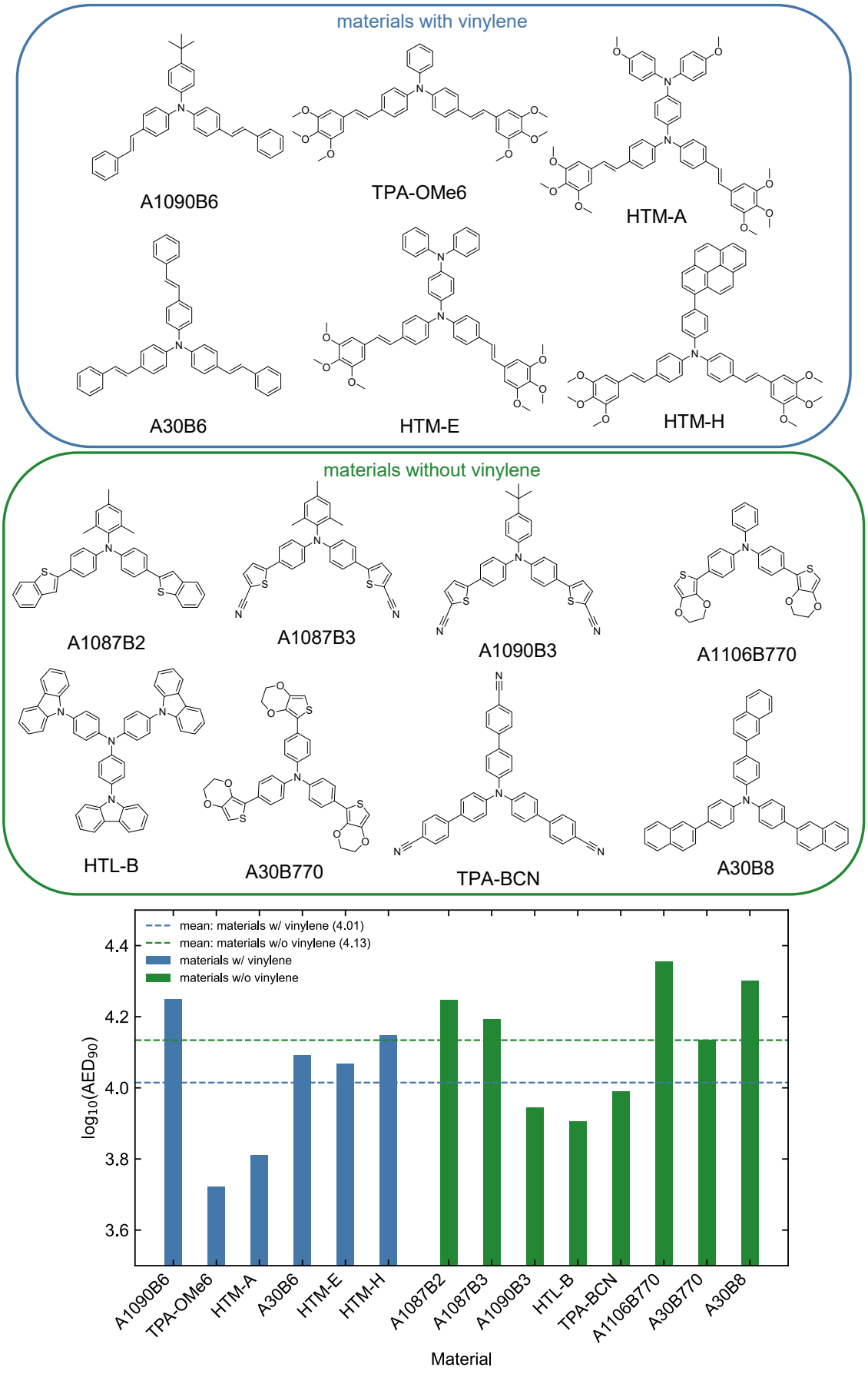

Figure S13: Comparison of gamma stability between materials with (blue) vs. without (green) vinylene groups.

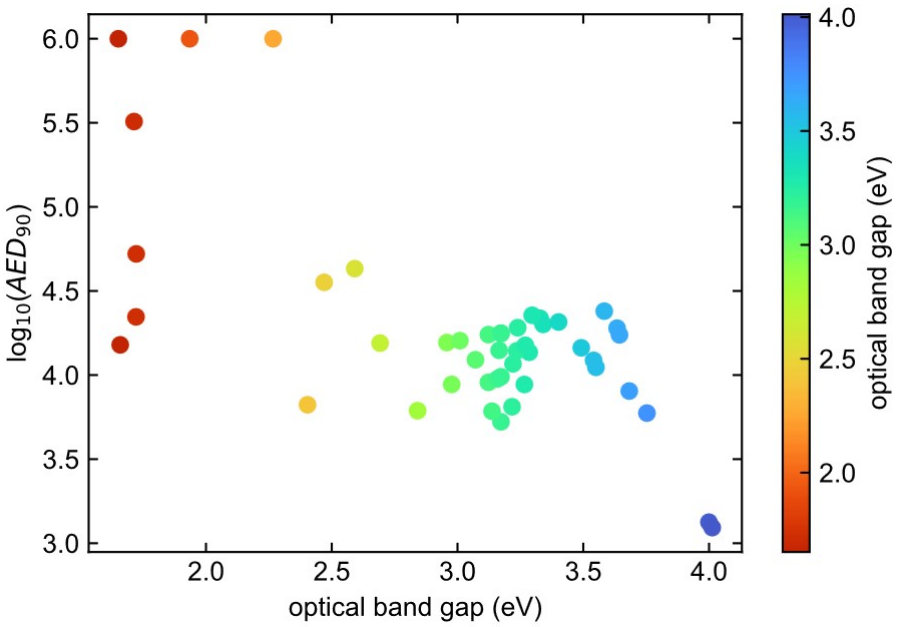

Figure S14: Dependence of the gamma stability target ($log_{10}(AED_{90})$) on the optical band gap. Most materials absorb in the blue or UV range, while BODIPY molecules absorb in the red.

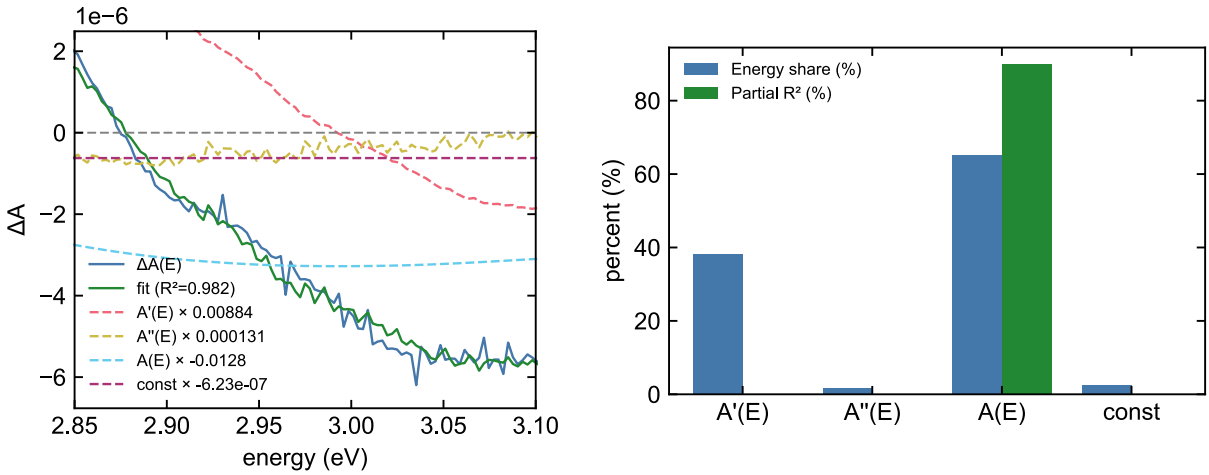

Figure S15: Stark derivative fit of ΔA(E) (4500–0 Gy, 2.85–3.10 eV) (left) and corresponding component contributions (right), showing dominance of A(E) and A'(E) with only minor A''(E) involvement.

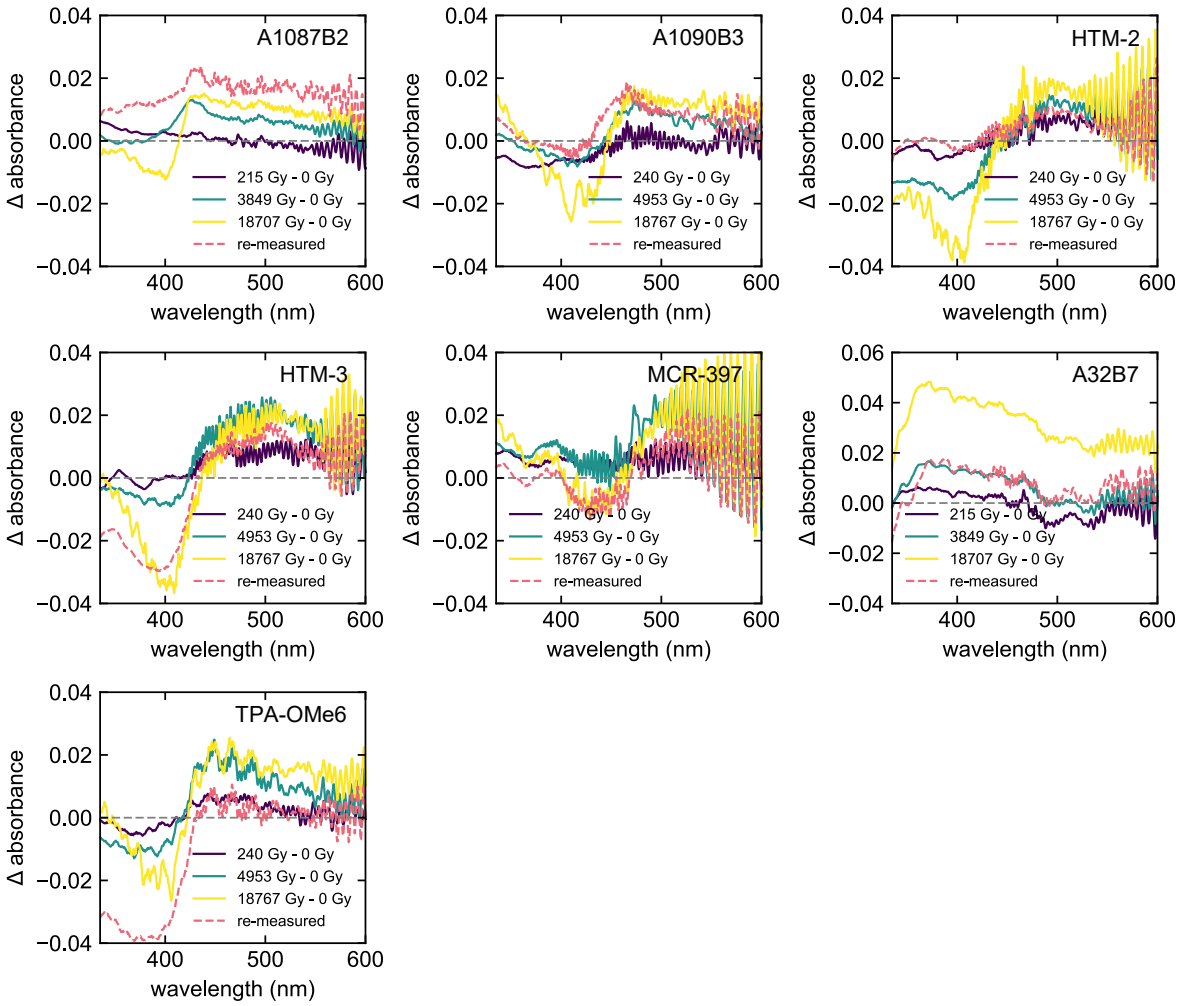

Figure S16: Differential absorbance spectra of materials showing an absorbance increase at low energies during gamma degradation. The red curves refer to re-measurements 10 months after degradation, investigating recovery. All curves were offset to y=0 by subtracting the average in the 900 nm – 1040 nm wavelength interval.

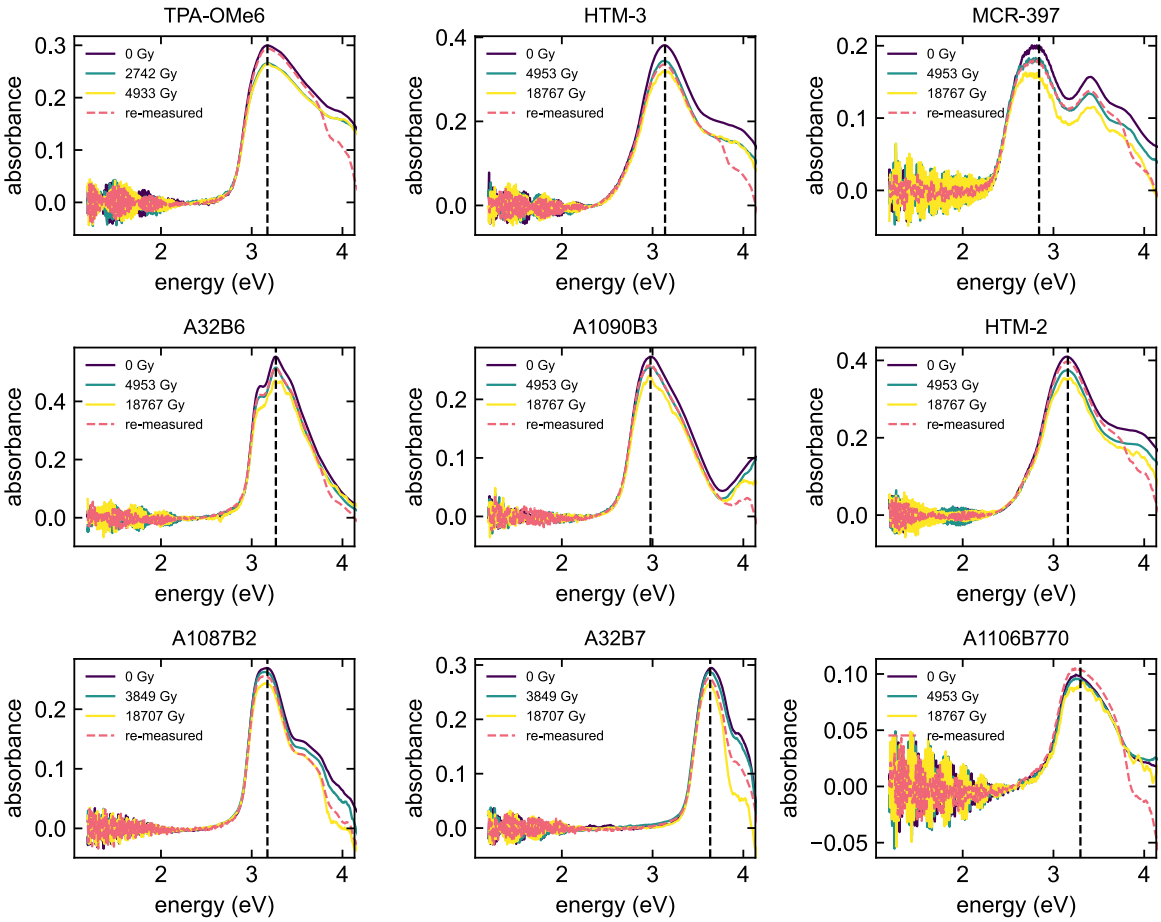

Figure S17: Baseline corrected UV-vis evolutions (Figure S9) of materials showing up to full recovery of their main π-π absorbance band (black line) 10 months after degradation (red curve). Due to low signal at high energies of the measurement equipment configuration used for the re-measurements, only signal at >335 nm (<3.7 eV) is trust-worthy.*

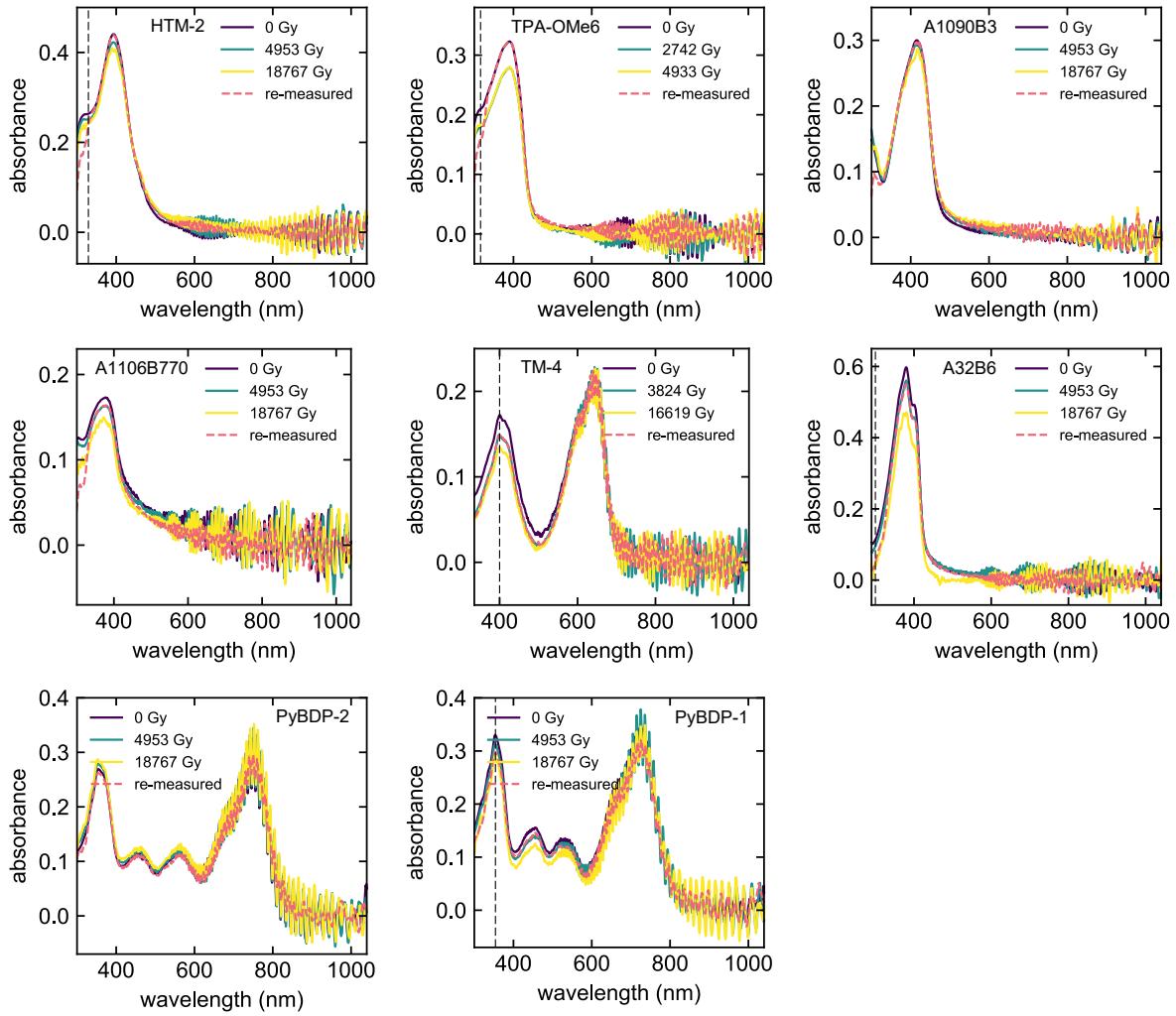

Figure S18: UV-vis evolutions of materials of materials showing up to full recovery of their main π-π absorbance band 10 months after gamma degradation (red curve) sorted by descending degree of recovery. Materials HTM-2, TPA-OMe6, TM-4, A32B6 and PyBDP-1 show an absorbance decrease at high energies (black line). For HTM-2, TM-4 and PyBDP-1, a recovery at high energies is observable within the possible measurement/transparency range of the re-measurement. Due to low signal at high energies of the measurement equipment configuration used for the re-measurements, only signal at >335 nm is trust-worthy. All curves were offset to y=0 by subtracting the average in the 900 nm – 1040 nm wavelength interval.*

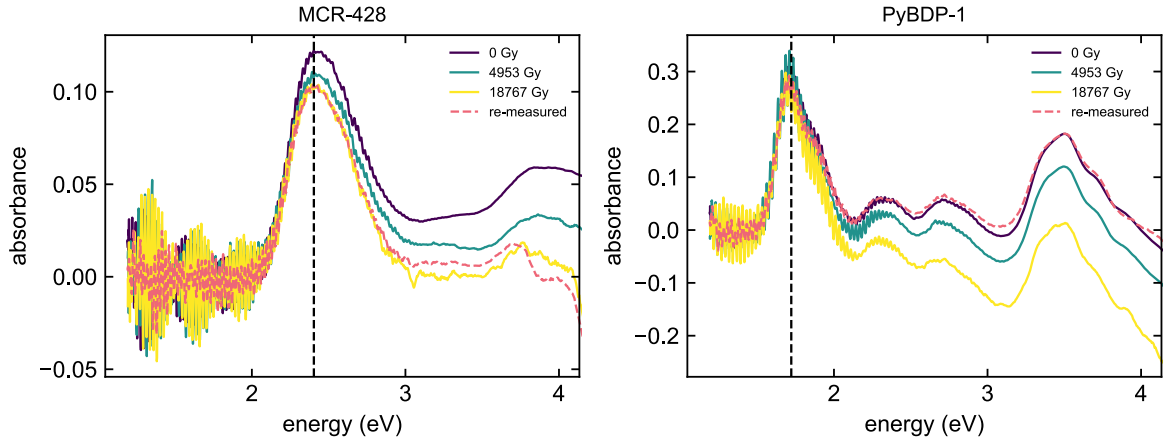

Figure S19: Baseline corrected UV-vis evolutions (Figure S9) of the 2 out of 16 re-measured materials showing no recovery of their main π-π absorbance band (black line) 10 months after degradation (red curve).*

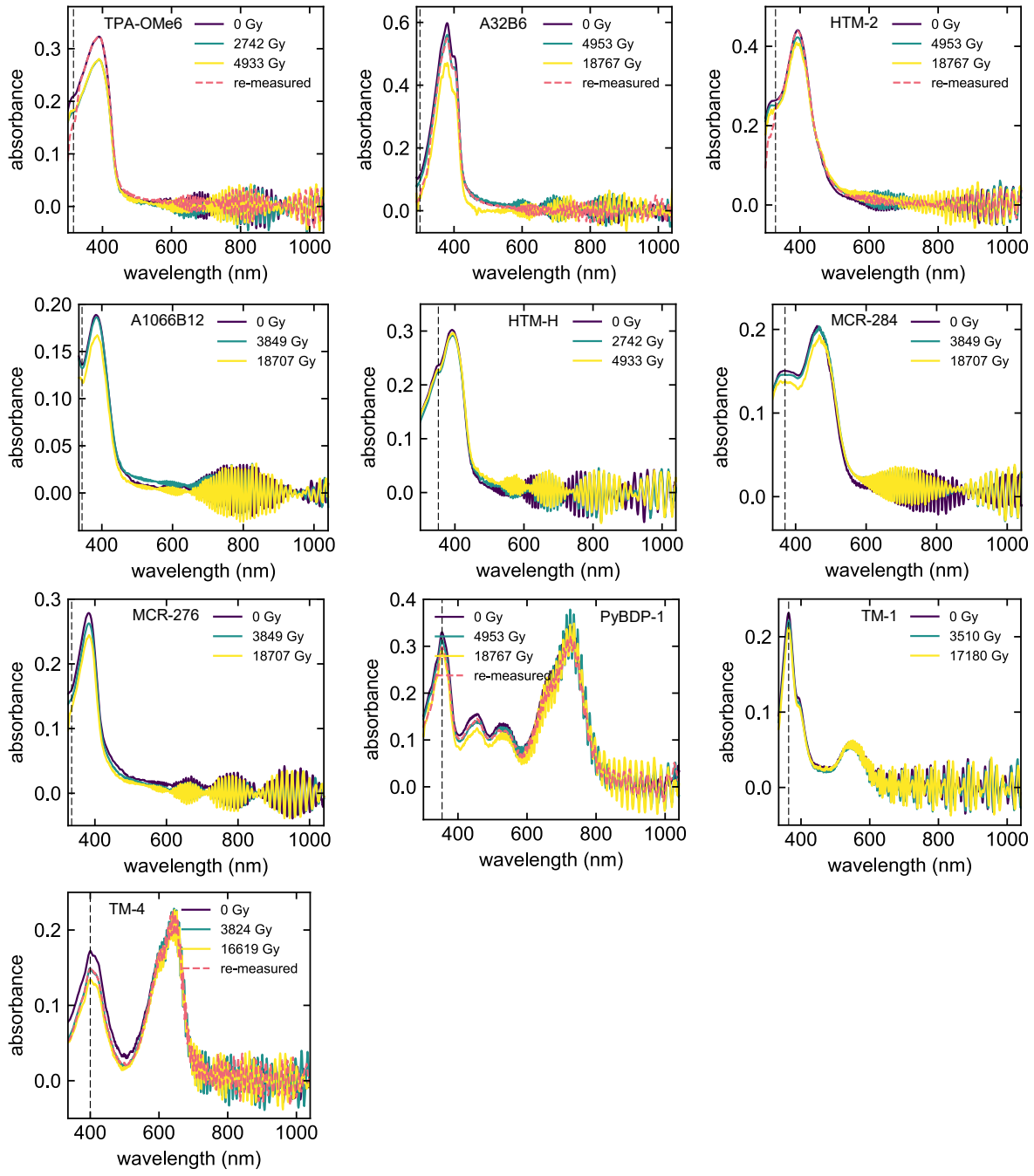

Figure S20: UV-vis evolutions of materials showing an absorbance decrease at high energies (black line). The $\Delta A/A_0$ values used in the lower panel of Figure 5b are extracted at the position of the black line, where A_0 refers to the UV-vis spectrum before degradation (purple curve) and ΔA is determined by calculating the difference between the UV-vis spectra before (purple curve) and after (yellow curve) gamma degradation. For HTM-2, TM-4 and PyBDP-1, a recovery at high energies is observable within the possible measurement/transparency range of the re-measurement. Due to low signal at high energies of the measurement equipment configuration used for the re-measurements, only signal at >335 nm is trust-worthy. All curves were offset to y=0 by subtracting the average in the 900 nm – 1040 nm wavelength interval.

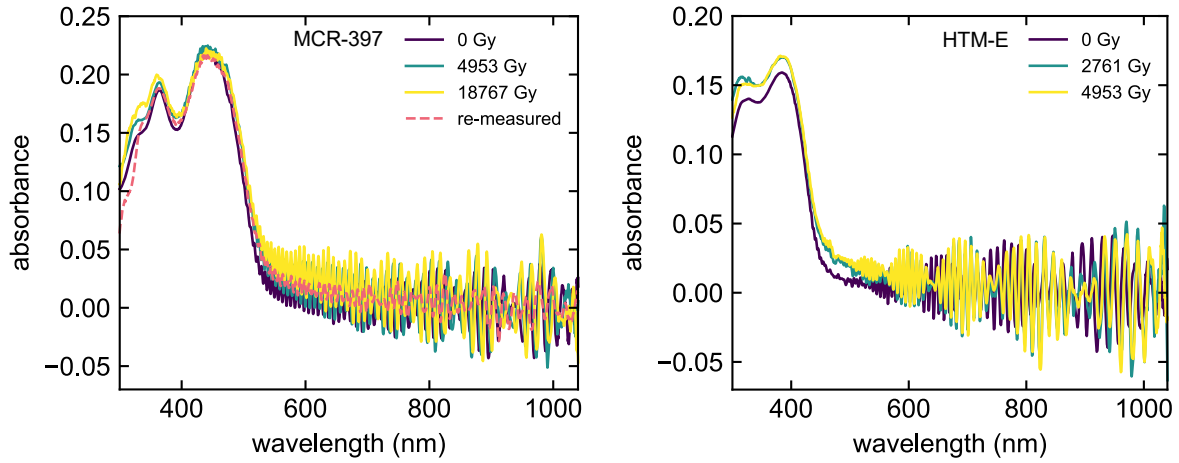

Figure S21: UV-vis spectra evolutions of materials showing an increase of absorbance throughout the whole spectral range during gamma degradation which could be associated with Rayleigh scattering. MCR-397 shows a recovery of the signal at both low and high energies in the re-measurement 10 months after degradation (red curve). Due to low signal at high energies of the measurement equipment configuration used for the re-measurements, only signal at >335 nm is trust-worthy. All curves were offset to y=0 by subtracting the average in the 900 nm – 1040 nm wavelength interval.

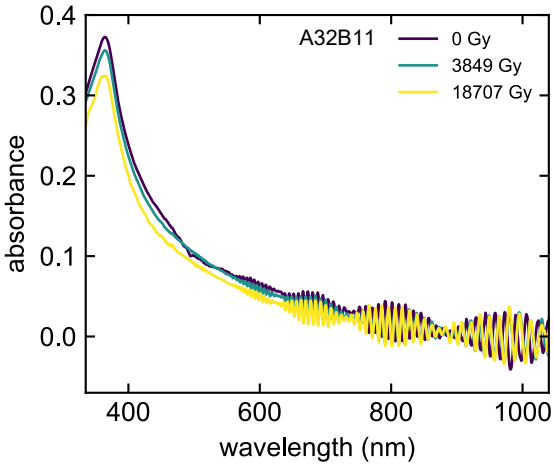

Figure S22: UV-vis evolution of material A32B11 showing a slowly declining baseline before degradation which could be associated with Mie scattering. During gamma degradation, the absorbance of the whole spectrum decreases. All curves were offset to y=0 by subtracting the average in the 900 nm – 1040 nm wavelength interval.

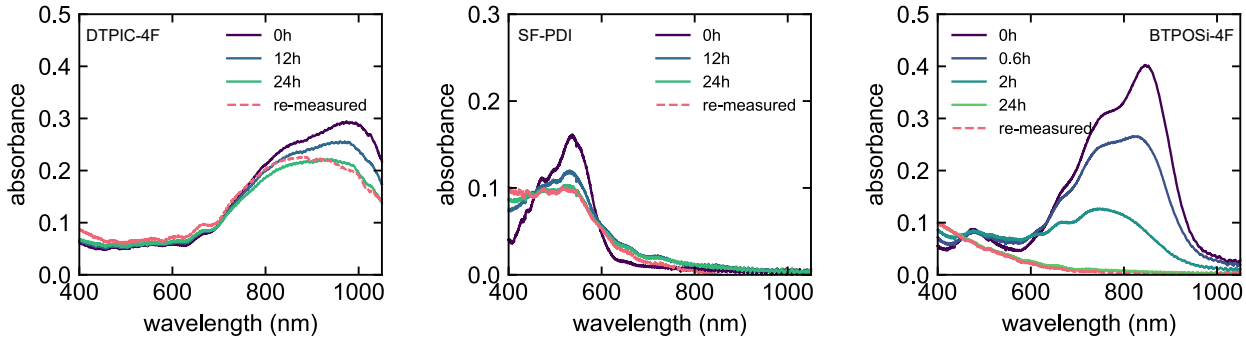

Figure S23: UV-vis evolutions of three organic semiconductors degraded with UVC light and re-measurement (red curve) 6 months after irradiation. A recovery of the π-π band is not evident for UVC degradation.*

References

1 J. Wu, J. Zhang, M. Hu, P. Reiser, L. Torresi, P. Friederich, L. Lahn, O. Kasian, D. M. Guldi, M. E. Pérez-Ojeda, A. Barabash, J. S. Rocha-Ortiz, Y. Zhao, Z. Xie, J. Luo, Y. Wang, S. I. Seok, J. A. Hauch and C. J. Brabec, *J. Am. Chem. Soc.*, 2023, **145**, 16517–16525.

2 J. Wu, L. Torresi, M. Hu, P. Reiser, J. Zhang, J. S. Rocha-Ortiz, L. Wang, Z. Xie, K. Zhang, B. Park, A. Barabash, Y. Zhao, J. Luo, Y. Wang, L. Lüer, L.-L. Deng, J. A. Hauch, D. M. Guldi, M. E. Pérez-Ojeda, S. I. Seok, P. Friederich and C. J. Brabec, *Science*, 2024, **386**, 1256–1264.

3 J. S. Rocha-Ortiz, J. Wu, J. Wenzel, A. J. Bornschlegl, J. D. Perea, S. Leon, A. Barabash, A.-S. Wollny, D. M. Guldi, J. Zhang, A. Insuasty, L. Lüer, A. Ortiz, A. Hirsch and C. J. Brabec, *Adv. Funct. Mater.*, 2023, **33**, 2304262.

4 I. Seoneray, J. Wu, J. S. Rocha-Ortiz, A. J. Bornschlegl, A. Barabash, Y. Wang, L. Lüer, J. Hauch, A. García, J. Zapata-Rivera, C. J. Brabec and A. Ortiz, *Sol. RRL*, 2024, **8**, 2400225.

5 M. Caicedo-Reina, J. S. Rocha-Ortiz, J. Wu, A. J. Bornschlegl, S. Leon, A. Barabash, J. Dario Perea, Y. Wang, V. Arango-Marín, A. Ortiz, L. Lüer, J. A. Hauch, B. Insuasty and C. J. Brabec, *Chem. – Eur. J.*, 2025, **31**, e202404251.

6 M. Caicedo-Reina, R. R. Guimarães, A. Ortiz, K. Araki and B. Insuasty, *J. Mol. Struct.*, 2022, **1251**, 132072.

7 *Standard practice for using the Fricke dosimetry system, ISO/ASTM 51026:2015*, ISO; ASTM International, Geneva; West Conshohocken, PA, 2015.

8 A. J. Bornschlegl, P. Duchstein, J. Wu, J. S. Rocha-Ortiz, M. Caicedo-Reina, A. Ortiz, B. Insuasty, D. Zahn, L. Lüer and C. J. Brabec, *J. Am. Chem. Soc.*, 2025, **147**, 1957–1967.

9 Schrödinger Release 2021-3; Maestro, Schrödinger, LLC, New York, NY (version Release 2021-3) Schrödinger, Inc., New York, NY 2021.

10 H. Moriwaki, Y.-S. Tian, N. Kawashita and T. Takagi, *J. Cheminformatics*, 2018, **10**, 4.

11 RDKit Release 2025.03.6 (version 2025.03.6) https://www.rdkit.org 2025.